Molecular Dynamics Simulations of Multilayer Polyelectrolyte Films: Effect of Electrostatic and Short-Range Interactions

Pritesh A. Patel,[†] Junhwan Jeon,[‡] Patrick T. Mather,[†] and Andrey V. Dobrynin*,[§,||]

Department of Macromolecular Science and Engineering, Case Western Reserve University, Cleveland, Ohio 44106, Department of Chemical Engineering, Vanderbilt University, Nashville, Tennessee 37235, and Polymer Program, Institute of Materials Science, and Department of Physics, University of Connecticut, Storrs, Connecticut 06269

Received June 9, 2006. In Final Form: September 1, 2006

The effect of the strength of electrostatic and short-range interactions on the multilayer assembly of oppositely charged polyelectrolytes at a charged substrate was studied by molecular dynamics simulations. The multilayer buildup was achieved through sequential adsorption of charged polymers in a layer-by-layer fashion from dilute polyelectrolyte solutions. The strong electrostatic attraction between oppositely charged polyelectrolytes at each deposition step is a driving force behind the multilayer growth. Our simulations have shown that a charge reversal after each deposition step is critical for steady multilayer growth and that there is a linear increase in polymer surface coverage after the first few deposition steps. Furthermore, there is substantial intermixing between chains adsorbed during different deposition steps. We show that the polymer surface coverage and multilayer structure are each strongly influenced by the strength of electrostatic and short-range interactions.

1. Introduction

The layer-by-layer (LbL) deposition of charged molecules is commonly used for fabrication of molecularly layered (2−10 nm per bilayer) multicomponent films with a high degree of complexity (see for review refs 1−9). The key to successful deposition of multilayer assembly in a layer-by-layer fashion is the charge inversion and subsequent reconstruction of surface properties that should occur after each adsorption step. A typical experimental procedure involves immersing a solid substrate into dilute solutions of anionic (or cationic) polyelectrolytes for an optimal period of time, followed by a rinsing step to remove any loosely adsorbed material. Continued film growth is achieved by alternating the deposition of polyanions and polycations from their aqueous solutions. After a few dipping cycles, experiments generally show a linear increase of multilayer thickness or mass, indicating that the process reaches a steady-state regime of growth.[1,5,10−14]

The local structure of multilayers formed by flexible polyelectrolytes is believed to be similar to that of bulk polyelectrolyte complexes formed between similar polymers.[15] Polyelectrolytes in two-component films are not stratified into well-defined layers but are intermixed over several adjoining layers.[1,2,16] Furthermore, there is a correlation between the salt-induced phase separation of polyelectrolyte complexes in solutions and multilayer assembly of these polyelectrolytes at surfaces,[6,17,18] such that one can control the multilayer assembly by changing the salt concentration and fraction of charged monomers on the polymer backbone. In the region of stable multilayer growth an approximately linear dependence of the layer thickness on salt concentration has been observed. However, the layer thickness and polymer surface coverage can also show nonmonotonic dependences on salt concentration. In these cases both the layer thickness and the amount of adsorbed polymers decrease with increasing salt concentration, indicating layer *disassembly*—formation of soluble polyelectrolyte complexes in solution.

Despite the extensive experimental studies of layer-by-layer deposition of charged molecules,[3,6,8,9,19−21] a theoretical understanding of such systems is lagging behind.[22−26] Solis and de la Cruz[22] have developed a model of spontaneous equilibrium

[†] Case Western Reserve University.

[‡] Vanderbilt University.

[§] Polymer Program, Institute of Materials Science, University of Connecticut.

[||] Department of Physics, University of Connecticut.

(1) Decher, G. Polyelectrolyte Multilayers, an Overview. In *Multilayer Thin Films*; Decher, G., Schlenoff, J. B., Eds.; Wiley-VCH: New York, 2003; pp 1−46.

(2) Decher, G. *Science* **1997**, *277*, 1232−1237.

(3) Hammond, P. T. *Curr. Opin. Colloid Interface Sci.* **1999**, *4*, 430−442.

(4) Kotov, N. A. Layer-by-Layer Assembly of Nanoparticles and Nanocolloids: Intermolecular Interactions, Structure and Materials Perspectives. In *Multilayer Thin Films*; Decher, G., Schlenoff, J. B., Eds.; Wiley-VCH: New York, 2003; pp 207−244.

(5) Schlenoff, J. B. Charge Balance and Transport in Polyelectrolyte Multilayers. In *Multilayered Thin Films*; Decher, G., Schlenoff, J. B., Eds.; Wiley-VCH: New York, 2003; pp 99−132.

(6) Sukhishvili, S. A. *Curr. Opin. Colloid Interface Sci.* **2005**, *10*, 37−44.

(7) Sukhorukov, G. B.; Fery, A.; Mohwald, H. *Prog. Polym. Sci.* **2005**, *30*, 885−897.

(8) Decher, G. Multilayer films (polyelectrolytes). *The polymeric materials encyclopedia: synthesis, properties and applications*; CRC Press: Boca Raton, FL, 1996; pp 4540−4546.

(9) Decher, G.; Eckle, M.; Schmitt, J.; Struth, B. *Curr. Opin. Colloid Interface Sci.* **1998**, *3*, 32−39.

(10) Decher, G.; Lvov, Y.; Schmitt, J. *Thin Solid Films* **1994**, *244*, 772−777.

(11) Kellogg, G. J.; Mayes, A. M.; Stockton, W. B.; Ferreira, M.; Rubner, M. F.; Satija, S. K. *Langmuir* **1996**, *12*, 5109−5113.

(12) Korneev, D.; Lvov, Y.; Decher, G.; Schmitt, J.; Yaradaikin, S. *Physica B* **1995**, *213*, 954−956.

(13) Losche, M.; Schmitt, J.; Decher, G.; Bouwman, W. G.; Kjaer, K. *Macromolecules* **1998**, *31*, 8893−8906.

(14) Lvov, Y.; Decher, G.; Haas, H.; Mohwald, H.; Kalachev, A. *Physica B* **1994**, *198*, 89−91.

(15) Kabanov, V. Fundamentals of polyelectrolyte complexes in solution and the bulk. In *Multilayer Thin Films*; Decher, G., Schlenoff, J. B., Eds.; Wiley-VCH: New York, 2003; pp 47−86.

(16) Schlenoff, J. B.; Dubas, S. T. *Macromolecules* **2001**, *34*, 592−598.

(17) Izumrudov, V.; Kharlapieva, E.; Sukhishvili, S. A. *Macromolecules* **2004**, *37*, 8400−8406.

(18) Kovacevic, D.; van der Burgh, S.; de Kaizer, A.; Cohen Stuart, M. A. *Langmuir* **2002**, *18*, 5607−5612.

(19) Schonhoff, M. *Curr. Opin. Colloid Interface Sci.* **2003**, *8*, 86−95.

(20) Schonhoff, M. *J. Phys.: Condens. Matter* **2003**, *15*, R1781−R1808.

(21) *Multilayer Thin Films*; Wiley-VCH: New York, 2003.

(22) Solis, F. J.; de la Cruz, M. O. *J. Chem. Phys.* **1999**, *110*, 11517−11522.

(23) Netz, R. R.; Joanny, J. F. *Macromolecules* **1999**, *32*, 9013−9025.

(24) Castelnovo, M.; Joanny, J. F. *Langmuir* **2000**, *16*, 7524−7532.

(25) Park, S. Y.; Rubner, M. F.; Mayes, A. M. *Langmuir* **2002**, *18*, 9600−9604.

10.1021/la061658e CCC: $33.50
Published on Web 10/26/2006 PAGE EST: 8.6

layering of mixtures of positively and negatively charged polymers close to a charged wall due to their chemical incompatibility. Netz and Joanny[23] have proposed a scaling model of multilayer formation from semiflexible polyelectrolytes. However, this model lacks intermixing between polyelectrolyte chains in neighboring layers. Castelnovo and Joanny[24] have taken into account the strong interpenetration of polyelectrolyte chains in consecutive layers by incorporating complex formation between oppositely charged polyelectrolytes into self-consistent field equations, describing the polymer density profile in the adsorbed layers. The numerical solutions of the self-consistent field equations have been recently presented by Wang[27] and by Shafir and Andelman.[28] These calculations have shown that sufficiently strong short-range attraction between oppositely charged polymers is essential for the formation of multilayers.

The formation of ionic pairs between polyelectrolyte chains forming multilayers was taken into account by Park et al.[25] and by Lefaux et al.[26] These models show promising results by predicting the correct salt concentration dependence of multilayer growth by sequential adsorption and by spin-coating methods. However, these models neglect strong intermixing between layers by assuming the frozen layer structure after completion of each deposition step. Such an assumption can only be justified for description of processes such as multilayer assembly by spin-coating[26] wherein chains do not have sufficient time to diffuse inside the film over the course of film assembly.

Multilayer assembly has also been studied by molecular simulations.[29−36] Messina et al.[29−31] have performed Monte Carlo simulations to study multilayer formation from mixtures of oppositely charged polyelectrolytes near charged spherical particles and at uniformly charged surfaces. These papers tested the hypothesis that multilayering is an equilibrium state and that it occurs whether one proceeds in a stepwise fashion, as envisaged in experiments, or one adds together oppositely charged polyelectrolytes and exposes the solution to a charged substrate. It was shown that additional short-range attractive interactions between polyelectrolytes and the surface are required to successfully initiate film growth. Unfortunately, these simulations were limited to the formation of only a couple layers for which the appearance of the charged oscillations might be the result of relaxation of polymer density fluctuations caused by the adsorbing surface. We note that no experiments have been reported showing the formation of multilayer thin films by dipping a charged substrate into premixed polyelectrolyte solutions.

Molecular dynamics (MD) simulations of the sequential adsorption of oppositely charged polyelectrolytes onto a charged spherical particle were performed by Panchagnula et al.[32,33] These simulations confirmed that the layer buildup proceeds through surface overcharging during each deposition step and with the system reaching a steady-state regime after a few deposition steps with nonlinear growth of the polymer mass in the aggregate. However, despite the steady growth, the spherical symmetry of such a macro-ion precluded formation of the well-developed multilayer structures and instead showed nonsymmetric oscillation of the local polymer composition—the density difference between positively and negatively charged chains within the polymeric film.

Multilayer formation on the planar surfaces was studied in molecular dynamic simulations of Patel et al.[34] These simulations have shown that the film buildup follows a linear growth pattern, with both the thickness of the adsorbed layer and polymer surface coverage increasing linearly with the number of deposition steps. This steady-state linear growth regime is generally observed in experiments after deposition of the first few layers.[3,6,8,9,19−21] For partially charged chains with $f = 1/2$ and $1/3$ (here, f is the fraction of charged beads in a bead−spring chain), the growth rate of the polymer surface coverage is higher than for the case of fully charged chains. This is in agreement with experimental observations of the thicker layers for partially charged polyelectrolytes compared to very thin layers obtained for the fully charged polymers. While simulations further showed strong intermixing between polyelectrolyte chains adsorbed during different deposition steps, almost perfect periodic oscillations in local polymer composition were observed, indicating polymer stratification.

Results of the molecular dynamics simulations of layer-by-layer assembly of polyelectrolytes and nanoparticles from dilute solutions have been reported by Jeon et al.[35] They have found that, for multilayer films consisting of nanoparticles, there is better stratification of the layers with almost constant thickness of the layer composed of nanoparticles. For all studied systems, the process of multilayer formation occurs over several successive deposition steps: usually four deposition steps are required to complete formation of the two layers. The film thickness and surface coverage increase almost linearly with the number of deposition steps, indicating steady-state film growth, while multilayered films formed by nanoparticles feature higher roughness than films consisting of flexible polymers.

In this paper, we use molecular dynamics simulations to study the effect of electrostatic and short-range interactions on multilayer assembly of oppositely charged polyelectrolytes at a charged planar surface. Simulations are performed using sequential adsorption of polyelectrolytes up to 10 deposition steps. The rest of the paper is organized as follows. Section 2 describes the model and simulation details. In section 3, we present simulation results with a detailed discussion of the evolution of the surface coverage, polymer density profile, and surface overcharging during the deposition process. Finally, in section 4 we summarize our results.

2. Model and Simulation Details

The MD simulations of multilayer assembly were performed from dilute polyelectrolyte solutions of bead−spring chains with degree of polymerization, N_p, equal to 32, 16, and 8. Each beadlike monomer has a diameter σ. For each degree of polymerization, the fraction of charged monomers on each chain was equal to $f = 1$ or $1/2$, corresponding to cases of completely charged or alternately (every other bead) charged polyelectrolytes, respectively. The connectivity of the beads within each chain is governed by the finitely extensible nonlinear elastic (FENE) potential:[37]

$$U_{\mathrm{FENE}}(r) = -0.5k_s{R_{\max}}^2 \ln(1 - r^2/{R_{\max}}^2) \qquad (1)$$

with the spring constant $k_s = 30k_BT/\sigma^2$, where k_B is the Boltzmann

(26) Lefaux, C. J.; Zimberlin, J. A.; Dobrynin, A. V.; Mather, P. T. *J. Polym. Sci., Part B: Polym. Phys.* **2004**, *42*, 3654−3666.
(27) Wang, Q. *J. Phys. Chem. B* **2006**, *110*, 5825−5828.
(28) Shafir, A.; Andelman, D. *Eur. Phys. J. E* **2006**, *19*, 155−162.
(29) Messina, R. *Langmuir* **2003**, *19*, 4473−4482.
(30) Messina, R.; Holm, C.; Kremer, K. *J. Polym. Sci., Part B: Polym. Phys.* **2004**, *42*, 3557−3570.
(31) Messina, R. *Macromolecules* **2004**, *37*, 621−629.
(32) Panchagnula, V.; Jeon, J.; Dobrynin, A. V. *Phys. Rev. Lett.* **2004**, *93*, 037801-1−4.
(33) Panchagnula, V.; Jeon, J.; Rusling, J. F.; Dobrynin, A. V. *Langmuir* **2005**, *21*, 1118−1125.
(34) Patel, P. A.; Jeon, J.; Mather, P. T.; Dobrynin, A. V. *Langmuir* **2005**, *21*, 6113−6122.
(35) Jeon, J.; Panchagnula, V.; Pan, J.; Dobrynin, A. V. *Langmuir* **2006**, *22*, 4629−4637.
(36) Abu-Sharkh, B. *J. Chem. Phys.* **2005**, *123*, 114907-1−114907-6.
(37) Frenkel, D.; Smit, B. *Understanding Molecular Simulations*; Academic Press: San Diego, 2001.

Table 1. Interaction Parameters and System Sizes

interaction parameter	system A	system B	system C	system D
l_B, Bjerrum length	3.0σ	1.0σ	3.0σ	1.0σ
monomer−monomer	$\epsilon_{LJ} = 0.3k_BT$ $r_{cut} = 2.5\sigma$	$\epsilon_{LJ} = 0.3k_BT$ $r_{cut} = 2.5\sigma$	$\epsilon_{LJ} = 1.0k_BT$ $r_{cut} = 2.5\sigma$	$\epsilon_{LJ} = 1.0k_BT$ $r_{cut} = 2.5\sigma$
surface bead−monomer belonging to positively charged chains	$\epsilon_{LJ} = 1.0k_BT$ $r_{cut} = 2^{1/6}\sigma$	$\epsilon_{LJ} = 1.0k_BT$ $r_{cut} = 2^{1/6}\sigma$	$\epsilon_{LJ} = 1.0k_BT$ $r_{cut} = 2.5\sigma$	$\epsilon_{LJ} = 1.0k_BT$ $r_{cut} = 2.5\sigma$
surface bead−monomer belonging to negatively charged chains	$\epsilon_{LJ} = 1.0k_BT$ $r_{cut} = 2.5\sigma$	$\epsilon_{LJ} = 1.0k_BT$ $r_{cut} = 2.5\sigma$	$\epsilon_{LJ} = 1.0k_BT$ $r_{cut} = 2.5\sigma$	$\epsilon_{LJ} = 1.0k_BT$ $r_{cut} = 2.5\sigma$
monomer−counterion	$\epsilon_{LJ} = 1.0k_BT$	$\epsilon_{LJ} = 1.0k_BT$	$\epsilon_{LJ} = 1.0k_BT$	$\epsilon_{LJ} = 1.0k_BT$
counterion−counterion	$r_{cut} = 2^{1/6}\sigma$	$r_{cut} = 2^{1/6}\sigma$	$r_{cut} = 2^{1/6}\sigma$	$r_{cut} = 2^{1/6}\sigma$
simulation box size($x \times y \times z$)	$28\sigma \times 29.4\sigma \times 81\sigma$	$20\sigma \times 20.784\sigma \times 81\sigma$	$20\sigma \times 20.784\sigma \times 81\sigma$	$20\sigma \times 20.784\sigma \times 81\sigma$

constant and T is the absolute temperature, and the maximum bond length $R_{max} = 1.5\sigma$.

The solvent in our simulations is modeled as a continuum with a macroscopic dielectric constant ϵ. Counterions with diameter σ were explicitly included in our simulations. Electrostatic interaction between any two charged particles bearing charge valences q_i and q_j and separated by a distance r_{ij} is given by the Coulomb potential:

$$U_{Coul}(r_{ij}) = k_BT(l_Bq_iq_j/r_{ij}) \quad (2)$$

All charged particles in our simulations were monovalent ions with $q_i = \pm 1$. As seen in eq 2, the strength of the electrostatic interactions is characterized by the Bjerrum length, $l_B = e^2/\epsilon k_BT$, defined as the length scale at which the Coulomb interaction between two elementary charges, e, in a dielectric medium of dielectric constant ϵ is equal to the thermal energy, k_BT. In our simulations, the Bjerrum length, l_B, was equal to either 1.0σ or 3.0σ, the latter leading to relatively strong electrostatic forces.

All particles in the system interact through a truncated−shifted Lennard-Jones (LJ) potential:

$$U_{LJ}(r) = \begin{cases} 4\epsilon_{LJ}\left[\left(\frac{\sigma}{r}\right)^{12} - \left(\frac{\sigma}{r}\right)^{6} - \left(\frac{\sigma}{r_{cut}}\right)^{12} + \left(\frac{\sigma}{r_{cut}}\right)^{6}\right], & \text{for } r \le r_{cut} \\ 0, & \text{for } r > r_{cut} \end{cases} \quad (3)$$

The cutoff distance, r_{cut}, and the interaction parameter, ϵ_{LJ}, are used to control the solvent quality for the polymer backbone and hydrophilicity and hydrophobicity of the adsorbing surface. Table 1 summarizes the interaction parameters used in our simulations. The polymer−polymer LJ interaction parameters for systems A and B are close to those for Θ-solvent conditions for the polymer backbone, while the LJ parameters for systems C and D correspond to poor solvent conditions for the polymer backbone with a negative value of the monomeric second virial coefficient. Charged polymers in poor solvent conditions for the polymer backbone are also called hydrophobic polyelectrolytes. In systems A and B there is an additional short-range repulsion between positively charged chains and a substrate.

The positively charged adsorbing surface (located at $z = 0$) was modeled by a periodic, hexagonally packed lattice of spheres with diameter σ. Every second particle on the surface carried univalent charge. A similar but noncharged surface was located at the opposite side of the simulation box to prevent the chains from escaping. The system was periodic in two dimensions (x and y directions) with the box sizes listed in Table 1. The particle−particle particle-mesh (PPPM)[37] method for the slab geometry, with the correction term implemented in LAMMPS[38] using the sixth-order charge-interpolation scheme and estimated accuracy of 10^{-5}, was used for calculations of the electrostatic interactions. In this method the 2-D periodic images of the system are periodically replicated along the z direction with distance $L = 3L_z$ between their boundaries. This reduces the problem of calculation of the electrostatic interactions in the 2-D periodic system to those in a 3-D system. Note that in our simulations we have assumed that the substrate and solution have similar dielectric constants and ignored the effect of image charges that appear when adsorption occurs at the surface with dielectric properties different from those of the solution.

(38) Plimpton, S. *LAMMPS User's Manual*; Sandia National Laboratory: Albuquerque, NM, 2005.

Table 2. Number of Chains Added to the Simulation Box during Each Deposition Step

N_p	system A	system B	system C	system D
32	80	40	40	40
16	160	80	80	80
8	320	160	160	160

During each deposition step, simulations were carried out using a constant number of particles, volume, and temperature ensemble (NVT).[37] The constant temperature was achieved by coupling the system to a Langevin thermostat. In this case, the equation of motion of the ith particle is

$$m(d\vec{v}_i(t)/dt) = \vec{F}_i(t) - \xi\vec{v}_i(t) + \vec{F}_i^{R}(t) \quad (4)$$

where $\vec{v}_i$ is the bead velocity and $\vec{F}_i$ is the net deterministic force acting on the ith bead of mass m. $\vec{F}_i^{R}$ is the stochastic force with zero average value, $\langle\vec{F}_i^{R}(t)\rangle = 0$, and δ-functional correlations, $\langle\vec{F}_i^{R}(t)\vec{F}_i^{R}(t')\rangle = 6\xi k_BT\delta(t - t')$. The friction coefficient was set to $\xi = m/\tau_{LJ}$ using the standard LJ time, $\tau_{LJ} = \sigma(m/\epsilon_{LJ})^{1/2}$. The velocity Verlet algorithm with a time step $\Delta t = 0.01\tau_{LJ}$ was used for integration of the equations of motion (4).

The coarse-grained MD simulations of the multilayer assembly presented in this paper correspond to modeling of four classes of polymeric systems with different affinities between the polymeric pairs and the substrate. In the bead−spring representation of a polymer chain, each bead represents several chemical units. For example, if we assume that the value of the Bjerrum length, $l_B = 1\sigma$, used in our simulations is equal to the Bjerrum length in water at room temperature ($T = 298$ K), $l_B = 7.14$ Å, the monomer size is equal to 7.14 Å. This corresponds to approximately 2.9 monomers of sodium poly(styrenesulfonate) (NaPSS) with monomer size 2.5 Å and leads to a chain with degree of polymerization $N_p = 32$ being on the order of 100 monomers. For the same set of parameters the surface charge density used in our simulations corresponds to 0.18 C/m^2.

Simulations were performed using the following protocol.[33,34] First, counterions from the charged surface were uniformly distributed over the box volume. Then, M_1 negatively charged polyelectrolytes (the number of chains added to the simulation box is given in Table 2), each with N_p monomers, corresponding to a monomer concentration, c, of $0.038\sigma^{-3}$, together with their counterions, were added to the simulation box and simulations continued until completion of the first deposition step. After completion of the first simulation run ("dipping" or deposition step), unadsorbed polyelectrolyte chains were removed ("rinsing" step). Here, we separate the unadsorbed polyelectrolytes from the adsorbed ones using a cluster algorithm[34] with a cutoff radius equal to 1.2σ. A chain is considered to belong

to a cluster if it has at least one monomer within a distance of 1.2σ from any monomer belonging to a chain forming the cluster. The cluster analysis was performed by analyzing the matrix of distances between all monomers in the system. Additionally, between adsorption steps, the only counterions required to maintain the system's electroneutrality (compensating the excess charge in the growing polymeric layer) were kept in the simulation box.

At the beginning of the second deposition step, the simulation box is refilled with $M_2 = M_1$ (see Table 2) positively charged polyelectrolytes together with their counterions, the new polyelectrolytes being added to the same concentration of monomers as before, $0.038\sigma^{-3}$. This is followed by another adsorption simulation run and rinsing step as for the first step. We repeated these dipping and rinsing steps to simulate the buildup of 10 deposition steps, performing the MD simulations lasting 10^6 integration steps for each deposition step.

The duration of the simulation runs was optimized to reach a saturation of polymer surface coverage during each deposition step.[34] This was done by monitoring the polymer surface coverage, Γ, defined as the total number of adsorbed monomers normalized by the surface area of the charged planar surface, S, as a function of the number of integration (MD) steps for longer simulation runs lasting 3×10^6 integration steps. We performed these simulations for the systems of fully charged chains with degree of polymerization $N_p = 32$. For all cases there is relatively fast saturation in the adsorption amount (about 90%) during the first 5×10^4 integration steps. Hence, the duration of the simulation run for each deposition step was set to 10^6 integration steps, which is about 20 times longer than is necessary to achieve a saturation limit. In our simulations chain diffusion and relaxation obey Rouse dynamics for which the chain's relaxation time increases with the chain degree of polymerization N_p as N_p^2. Thus, the selected length of the simulation runs is also sufficient for shorter polyelectrolyte chains with degree of polymerization $N_p =$ 16 and 8 to reach the steady-state regime.

3. Results and Discussion

3.1. Growth of Polymer Surface Coverage. The polymer surface coverage, Γ, was found to increase with each deposition step with a trend that depended on the fraction of charged monomers on the polymer backbone and values of the interaction parameters (Figure 1). These plots confirm that the strength of the polymer−polymer interactions plays an important role in successful film growth. For the systems with a short-range interaction parameter between monomers close to that at the Θ-point for the polymer backbone (systems A and B), the growth in polymer surface coverage with each step was found to feature a strong N_p dependence. For partially charged polyelectrolyte chains with a fraction of charged monomers $f = 1/2$, only the longest polymer chains ($N_p = 32$) show steady film growth (see Figure 1a,b). A strong effect of short-range repulsion is also observed for fully charged chains, but it is less pronounced than for the systems of partially charged polyelectrolytes. This behavior is a result of competition between short-range repulsion and electrostatic attraction between oppositely charged chains. For the shortest chains with $N_p = 8$ the absolute value of the chain adsorption energy is 4 times *lower* than that for the longest chains with $N_p = 32$, making chain desorption more probable.

In comparison to systems A and B, hydrophobic polyelectrolytes (systems C and D) form stable films (see Figure 1c,d). In these cases, the steady-state regime was reached after completion of just the first few deposition steps, regardless of the charge fraction and degree of polymerization. This is supported by the linear growth of the polymer surface coverage with the number of deposition steps. We reason that the additional hydrophobic interactions ($\epsilon_{LJ} = 1.0$ vs $\epsilon_{LJ} = 0.3$) enhance the affinity between oppositely charged polyelectrolytes, strengthening chain associations within the multilayers. For partially charged chains with $f = 1/2$, the growth rate of polymer surface coverage was found to be higher than for the case of fully charged chains. In the case of partially charged chains, for each adsorbed charge there was one extra monomer added to the adsorbed layer.

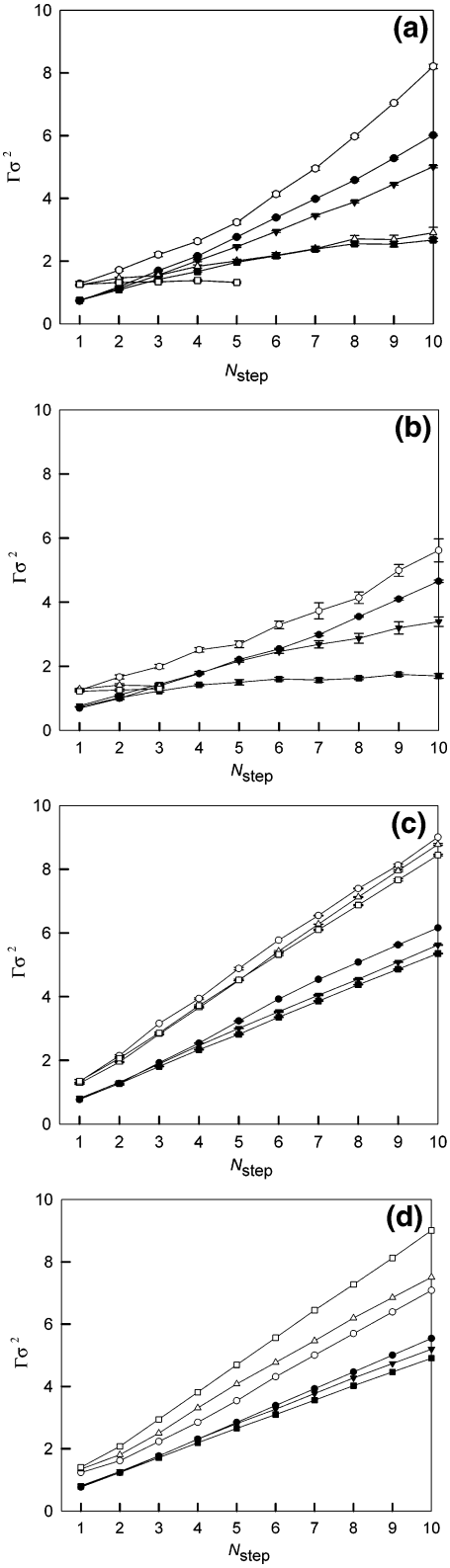

Figure 1. Dependence of the surface coverage (Γ) on the number of deposition steps for (a) system A, (b) system B, (c) system C, and (d) system D (see Table 1). The filled symbols are used for the fully charged chains ($f = 1$), and open symbols are for partially charged chains ($f = 1/2$). The degree of polymerization $N_p = 32$ (circles), 16 (triangles), and 8 (squares).

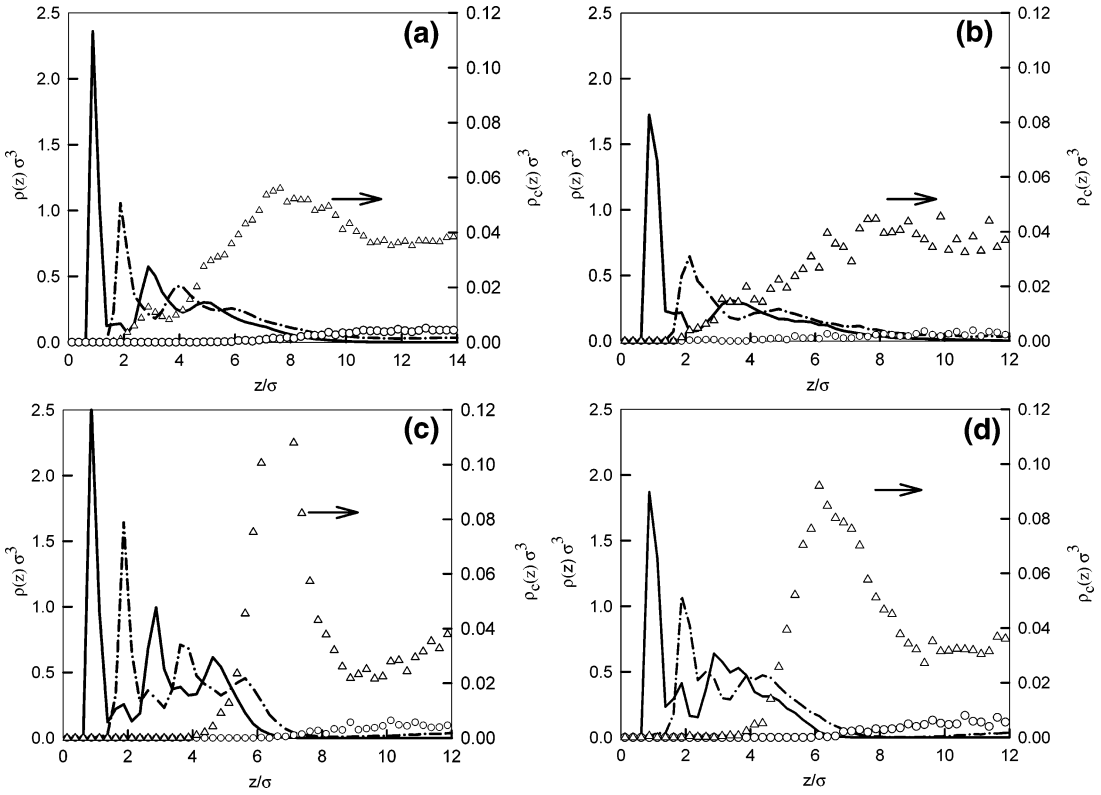

Figure 2. Polymer and counterion density distributions inside multilayers after completion of the eight deposition steps for systems of fully charged chains, $f = 1$, with degree of polymerization $N_p = 32$. The solid line shows the polymer density distribution of the negatively charged chains and the dashed−dotted line the polymer density distribution of positively charged chains. Open circles and triangles show density profiles of positively and negatively charged counterions, respectively. Key: (a) system A, (b) system B, (c) system C, (d) system D.

3.2. Distribution of Polymer Density. A density profile of monomers belonging to positively and negatively charged chains in the multilayers is shown in Figure 2. All data were collected during the eighth deposition step. The polymeric systems with weak short-range interactions (systems A and B, Figure 2a,b) show a less pronounced stratification than systems with additional short-range attractive interactions (systems C and D, Figure 2c,d). The monomer density of negatively charged chains for systems A and B, $\rho_-(z)$, shows two peaks near 1σ and 3σ. The well-developed peaks in the density profile of positively charged chains, $\rho_+(z)$, are located at 2σ and 4σ. The first peak near the surface is clearly larger than the other peaks. This is due to the high surface charge density of the initial substrate in comparison with the value of the surface overcharging achieved after completion of each deposition step. A larger number of adsorbed polyelectrolyte chains is required during the first deposition step to compensate for the surface charge while also overcharging the surface for subsequent layer buildup. A similar trend in higher polymer surface coverage of the surface layer is seen for hydrophobic polyelectrolyte systems as well (systems C and D, Figure 2c,d). However, these systems show more layers and better stratification between positive and negative polyelectrolytes in comparison with systems A and B. Thus, additional attraction between polyelectrolyte segments leads to better organized multilayered films. Such improved stratification between layers leads to the formation of a larger number of well-defined layers after completion of the same number of deposition steps for systems C and D.

The film composition, shown in Figure 2, supports the three-zone structure of the multilayer film.[21] Zone I contains the layer in the vicinity of the adsorbing surface with excess molecules carrying a charge opposite that of the substrate. The thickness of this layer depends on the electrostatic and short-range interactions between the polyelectrolyte chains and the substrate. Zone II contains complexes of oppositely charged macromolecules. Inside this zone polyelectrolytes are well intermixed and show 1:1 charge stoichiometry. This zone is wider for hydrophobic polyelectrolytes that also show sharper boundaries between different layers. The growth of the film occurs by increasing the thickness of zone II.

Zone III includes the outermost layer along with counterions, which neutralize the excess charge in the growing polymeric film. The counterions diffuse further into the polymeric film for the systems with repulsive short-range interactions (see Figure 2a,b); this correlates well with the lower polymer density inside the film. On the contrary, hydrophobic systems (Figure 2c,d) feature a counterion density profile that is narrow and has a large peak magnitude located just outside the ridge of the polymeric film. The exclusion of counterions from the film interior is a result of the higher polymer density and lesser amount of the free volume available for counterions inside multilayered films assembled from hydrophobic polyelectrolytes.

The average polymer density inside zone II—low for systems A and B and high for systems C and D—is controlled by the fine interplay between fluctuations/correlation-induced attraction between oppositely charged chains and excluded volume interaction between monomers.[39,40] To understand this, let us consider a concentrated polymer solution with correlation length ξ. At length scales smaller than the solution correlation length the chain statistics is unperturbed by fluctuation/correlation-induced attractive interactions, resulting in an usual scaling relation between the correlation length and g, the number of

(39) Dobrynin, A. V.; Colby, R.; Rubinstein, M. *J. Polym. Sci., Part B: Polym. Phys.* **2004**, *42*, 3513−3538.
(40) Grosberg, A. Y.; Nguyen, T. T.; Shklovskii, B. I. *Rev. Mod. Phys.* **2002**, *74*, 329−345.

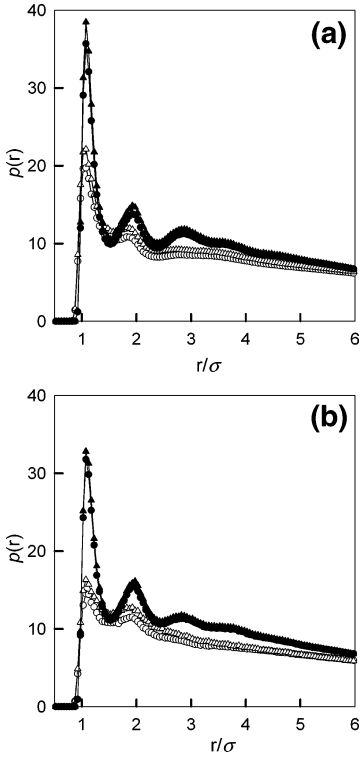

Figure 3. Correlation function between positively and negatively charged monomers inside multilayers formed by fully charged chains, $f = 1$, with degree of polymerizations $N_p = 32$ (circles) and 16 (triangles) after completion of the eight deposition steps: (a) systems A (open symbols) and C (filled symbols), (b) systems B (open symbols) and D (filled symbols).

constituent beads (monomers) in a correlation blob, $\xi \approx \sigma g^{1/2}$. For length scales larger than the correlation length, attractive interactions cause dense packing of the correlation blobs. The local structure of the melt of blobs resembles that of a concentrated solution, with each blob being surrounded by the oppositely charged blobs with higher probability. This structure of the adsorbed layer is supported by the charge−charge correlation function, $p(r)$, between positively and negatively charged monomers shown in Figure 3. This function is proportional to the probability of finding a negatively charged monomer at a distance r from a selected positively charged one.

The electrostatic interaction between any two neighboring oppositely charged blobs separated by a distance ξ is on the order of the thermal energy, k_BT:

$$-k_BT\frac{l_Bf^2g^2}{\xi} \approx -k_BT\frac{l_Bf^2g^{3/2}}{\sigma} \approx -k_BT \qquad (5)$$

This leads to the number of monomers in a blob and its size being equal to

$$g \approx (uf^2)^{-2/3} \quad \text{and} \quad \xi \approx \sigma(uf^2)^{-1/3} \qquad (6)$$

where u is the ratio of the Bjerrum length, l_B, to the bond length, $u = l_B/\sigma$. With increasing Bjerrum length (and thus increasing value of the parameter u), the blob size decreases, which is manifested in Figure 3 as growth and sharpening of the first maximum in the correlation function, $p(r)$.

The correlation blobs inside the film are space-filling, leading to the following expression for the average polymer density:

$$\rho\sigma^3 \approx \sigma^3 g/\xi^3 \approx (uf^2)^{1/3} \qquad (7)$$

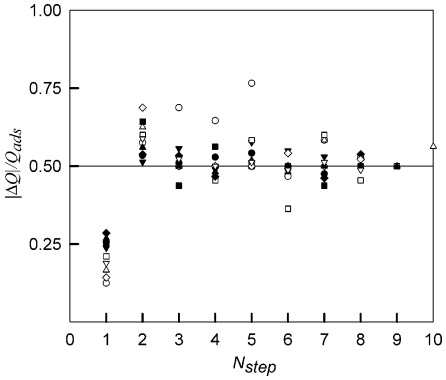

Figure 4. Dependence of the overcharging fraction ($|\Delta Q|/Q_{ads}$) on the deposition step number for different fractions of charged monomers, $f = 1$ (filled symbols) and $f = 1/2$ (open symbols), and degree of polymerization $N_p = 32$, 16, and 8: system A with $N_p = 32$ (circles), system A with $N_p = 16$ (inverted triangles), system B with $N_p = 32$ (triangles), system C with $N_p = 32$ (squares), system C with $N_p = 16$ (tilted squares), system C with $N_p = 8$ and $f = 1$ (filled triangles) and $f = 1/2$ (inverted open triangles).

The polymer density inside each layer increases with increasing strength of the electrostatic interactions. Note that the scaling analysis presented above can only be applied to describe the average film density for systems A and B for which the parameters of the LJ potential are close to that for a Θ-point. The ratios of the average polymer density in the middle of the polymeric film for systems A and B with $l_B = 3\sigma$ ($\rho(1)/\rho(0.5) \approx 1.48$) and $l_B = 1\sigma$ ($\rho(1)/\rho(0.5) \approx 1.52$) are close to the ratio $\rho(1)/\rho(0.5) = 2^{2/3} = 1.59$ obtained from eq 7.

For systems C and D the parameters of the LJ interactions correspond to poor solvent conditions for the polymer backbone. These systems do not show a strong effect of the Bjerrum length on the average polymer density such that for both systems it is close to $\rho\sigma^3 = 0.53$. This indicates that LJ interactions rather than fluctuation/correlation-induced attractive interactions control the average polymer density inside the polymeric film.

The weak dependence of the period of density oscillations, d, in the multilayered film on the fraction of charged monomers, f, can be rationalized in the framework of the scaling model presented in the Appendix. System A has an increase in the period d by a factor of 1.3 for a system with $f = 1/2$ in comparison with that for a system of fully charged chains. This increase is in agreement with predictions of eq A.4. For systems C and D the average polymer density is a constant and does not depend on f. In this case the period d is proportional to $f^{-1/2}$. This inverse square-root dependence of the period of density oscillations is in agreement with the factor of 1.32 increase of the parameter d seen in our simulations for system D with $f = 1/2$ in comparison with that for a system of fully charged chains.

3.3. Universality of the Film Growth. The growth of each layer in LbL growth occurs at the top of the polymeric film. To achieve steady-state LbL growth, the layer should be overcharged by the same amount at each step to recreate the surface properties. Indeed, this surface recreation was observed in our simulations, indicating universality among the systems studied. The universality of the overcharging process during steady-state film growth is shown in Figure 4. The ratio of the absolute value of the layer overcharging, $|\Delta Q|$, to the net charge carried by adsorbed chains at a given deposition step, $Q_{ads} = f(N(s) - N(s-1))$ (where $N(s)$ is the total number of adsorbed monomers after completion of the sth step), is plotted versus the number of deposition steps, N_{step}. This quantity is relatively independent of the fraction of charged monomers on the polymer backbone as well as the chain degree of polymerization. After several deposition steps, when

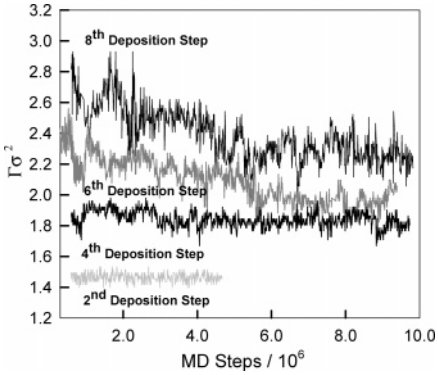

Figure 5. Time dependence of the polymer surface coverage for system A with fraction of charged monomers $f = 1/2$ and degree of polymerization $N_p = 16$ during the second, fourth, sixth, and eighth deposition steps.

the processes reach a steady state, this ratio approaches a value of 1/2 for all studied systems (see also refs 32−34). Thus, for steady-state growth, one charge is needed per excess ionic group to compensate for the surface charge while another is needed to recreate the surface properties for the adsorption of the next layer. Note that if this ratio is smaller than 1/2, the film eventually stops growing; if it is more than 1/2, the layer mass will show exponential growth. In both cases, the growth process is unstable. Fluctuations around this saturation value can be attributed to corresponding fluctuations in the number of adsorbed chains and should decrease with increasing system size. It is important to point out that surface overcharging plays two roles. First, it recreates the surface properties (primarily charge) for the next deposition layer, and second, it prevents the unrestricted growth of adsorbing polymers through electrostatic interactions between excess charges.

We can use eq A.7 to compare the ratio of the rates of change of the polymer surface coverage for systems B and D with partially and fully charged chains. For system B this ratio is equal to $\Delta\Gamma(0.5)/\Delta\Gamma(1) \propto 2^{1/6} \approx 1.12$, and for system D, $\Delta\Gamma(0.5)/\Delta\Gamma(1) \propto 2^{3/2} \approx 2.8$. In our simulations these values are close to 1.18 and 3, respectively. Thus, simulations show reasonable agreement with the scaling model described in the Appendix.

3.4. Stability of the Growing Film and Chain Exchange. To study film stability and chain exchange during multilayer assembly, we performed a longer molecular dynamics simulations of system A with $N_p = 16$ and $f = 1/2$. The selection of this system was dictated by the fact that it shows initial film growth that stops after the completion of the eighth deposition step (see Figure 1a). Thus, this system demonstrates both stable film growth at the initial stages of the deposition process and unstable film growth, with saturation in $\Gamma\sigma^2$ values, at the later stages. The initial configurations for these simulations were the final configurations of the simulation runs after completion of the second, fourth, sixth, and eight deposition steps. These simulations were continued for an additional 4×10^6 MD steps for the second deposition step and 9×10^6 MD steps for all other deposition steps. The time dependence of the polymer surface coverage during these longer simulation runs is shown in Figure 5. For the second and fourth deposition steps the polymer surface coverage fluctuates around an average value. The fluctuations increase in magnitude for the fourth deposition step in comparison with those during the second deposition step. Upon close inspection, we observed that this increase in amplitude of the fluctuations is due to a large number of negatively charged loops and the chain's ends dangling into solution after completion of the third deposition step. The fluctuations in the number of

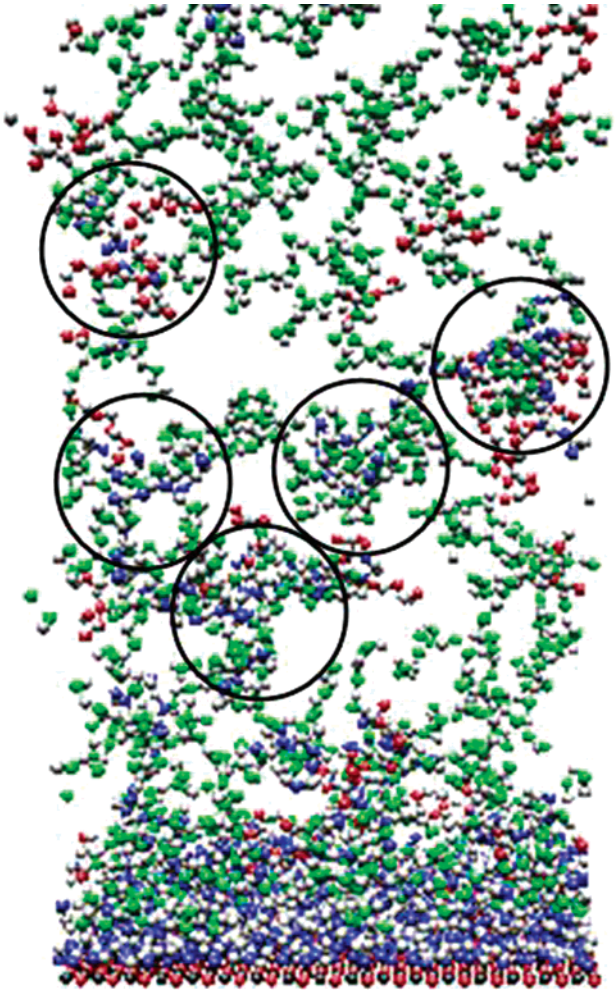

Figure 6. Snapshot of the simulation box during the extended simulation run of the eighth deposition step for system A with $N_p = 16$ and $f = 1/2$. Positively charged monomers on the polyelectrolyte chains are colored in red and green. The negatively charged monomers are shown in blue. The green bead chains are polyelectrolytes added during the eighth deposition step, while the red bead chains are previously adsorbed polyelectrolytes. Neutral beads on the chains are shown in gray, and those on the surface are shown in black.

contacts between these loops and positively charged chains in a solution are responsible for the variations in the polymer surface coverage seen in Figure 5.

A qualitatively different picture for the time dependence of the polymer surface coverage is observed during the longer simulations of the sixth and eighth deposition steps. For these deposition steps, the polymer surface coverage not only shows oscillations but also gradually decreases as the simulation runs continue. This decrease is associated with desorption of the negatively charged chains which were adsorbed during the previous deposition steps. The desorbed negatively charged chains can be seen in Figure 6 (blue beads), which presents a snapshot of the simulation box during the extended simulation run of the eighth deposition step. It is interesting to point out that these negatively charged chains form complexes with positively charged chains in a solution. These could be either 1:1 or 1:2 complexes. Furthermore, desorption of negatively charged chains occurs dynamically in conjunction with positively charged ones. The double-chain desorption process has a lower activation barrier (shown below) than desorption of a single negatively charged chain. Note that the single-chain desorption events are still possible but a desorbing negatively charged chain will immediately form a complex with a positively charged one. This happens already

during the escape process when part of the negatively charged chain is still buried inside the film.

As suggested above, there is a simple explanation for why the two-chain desorption process is more favorable than a single-chain event. For single-chain desorption, the activation barrier that chains should overcome to escape from the polymeric film is proportional to the absolute value of the chain's cohesion energy:

$$E_{act}^{(1)} \approx k_B T N_p \epsilon_{coh} \quad (8)$$

This activation energy is proportional to the chain's degree of polymerization because by desorbing a chain eliminates all favorable contacts with its surroundings inside the multilayer film. However, by desorbing in pairs, chains form a 1:1 complex whose interior structure is similar to that inside the multilayered film. Thus, only monomers located on the surface must break favorable attractive interactions. The activation energy for this process is proportional to the number of monomers on the surface of the complex, N_s, times the absolute value of the cohesive energy per monomer, ϵ_{coh}:

$$E_{act}^{(2)} \approx k_B T N_s \epsilon_{coh} \approx k_B T (N_p/g)^{2/3} \quad (9)$$

In writing eq 9, we used the scaling model described in section 3.2. The activation energy of the two-chain process is lower than that of the single-chain process, $N_s < N_p$. Equation 9 also explains why a single-chain desorption is always accompanied by complexation with an oppositely charged chain in a solution. Instead of eliminating all favorable contacts, the desorbing chain only loses part of them, N_s, by recreating the rest of them through complexation in solution with an oppositely charged chain.

Let us now estimate the N_p dependence of the characteristic time scale for chain desorption. In our simulations we used the Langevin thermostat to control the system temperature. Molecular dynamics simulations with the Langevin thermostat correspond to the Rouse chain dynamics.[42] In this case the chain relaxation time in a solution is proportional to N_p^2 so that the characteristic time scale for chain desorption is estimated as

$$\tau_{des} \approx \tau_0 N_p^2 \exp((N_p/g)^{2/3}) \quad (10)$$

where τ_0 is a characteristic monomeric time scale. Thus, the stable multilayer growth shown in Figure 1 could be argued to be a result of a slow chain desorption process that only happens for relatively short chains with weak attractive interactions. With increasing number of ionized groups, chain degree of polymerization, and chain hydrophobicity, chain desorption is slowed, favoring the formation of stable multilayered structures.

4. Conclusions

We have presented a molecular dynamics study of the effect of short-range and electrostatic interactions on sequential multilayer assembly at charged surfaces. Our simulations confirm the hypothesis that surface overcharging is crucial for stable film growth. Furthermore, steady-state multilayer growth strongly depends on the strength of the electrostatic and Lennard-Jones interactions. Those systems with LJ interaction parameters close to Θ-conditions for the polymer backbone (systems A and B) only show stable layer growth for systems with a sufficiently strong chain cohesive energy. This is indicated by the stable film growth for system A with $N_p = 32$ and $f = 1$ or 1/2 and $N_p = 16$ and $f = 1$ and for system B with $N_p = 32$ and $f = 1$ or 1/2. For shorter polymer chains, the activation barrier against chain desorption is sufficiently low to allow frequent chain desorption events. Interestingly, we observed that polyelectrolyte chains desorb in pairs and show that 1:1 complex stoichiometry minimizes the number of favorable ionic and monomer−monomer interactions to be broken during desorption.

In poor solvent (hydrophobic) conditions for the polymer backbone (systems C and D), the additional attractive LJ interactions improve the film stability, resulting in steady-state multilayer growth for all studied chain lengths. By improving the affinity between polymer chains, the activation barrier against chain desorption is increased. Furthermore, additional affinity between the polymer backbones improves layer stratification. Systems C and D witnessed faster growth (steeper slope) than systems A and B. Irrespective of interactions, partially charged chains were seen to allow higher polymer surface coverage than the fully charged ones.

Within the formed multilayers, positively charged monomers are surrounded by negatively charged monomers (see Figure 3a,b). This charge distribution is similar to the charge distribution found in polyelectrolyte complexes and inside the core of the diblock polyampholyte micelles.[39,43] The average polymer density inside the multilayers was shown to be a result of the fine interplay between electrostatic and short-range interactions, with systems in poor solvent conditions for the polymer backbone (systems C and D) being found to feature a higher average polymer density inside the multilayers.

The molecular simulations presented in this paper were limited to the case of flexible polyelectrolytes in a solvent modeled as a continuum. Modeling the solvent as a continuum eliminates an important effect of the size of the solvent molecules on the packing of polymer chains at the substrate as well as variations in the solution dielectric constant within the growing polymeric film. Another effect that we did not consider in our simulations is the effect of the chemical structure of the polyelectrolyte chains such as the chain rigidity and charge distribution along the polymer backbone on the chain complexation within the multilayered film. All these modifications of the model could lead to new features of multilayer assembly. We will address these issues in our future publications.

Acknowledgment. A.V.D. acknowledges funding from the National Science Foundation (Grant DMR-0305203). P.T.M. acknowledges funding from Ivoclar-Vivadent AG.

Appendix

The oscillations of the polymer composition in a concentrated mixture of positively and negatively charged chains (such as our multilayers (zone II); see Figure 2) are a result of competition between polymeric and electrostatic effects. Consider 1-D variations of the polymer composition along the z direction with period d and magnitude with respect to the average polymer density. The excess of the polymeric part of the system free energy per period d due to this density wave is given by the following equation:[34,41]

$$\Delta F_{pol} \approx k_B T S \int_0^d \frac{\sigma^2}{\rho(z)} \left(\frac{d\rho(z)}{dz}\right)^2 dz \approx k_B T S \frac{\sigma^2 \Delta\rho^2}{\rho d} \quad (A.1)$$

where S is the surface area. This variation of the polymer density

(41) Grosberg, A. Y.; Khokhlov, A. R. *Statistical Physics of Macromolecules*; AIP Press: New York, 1994.

(42) Doi, M.; Edwards, S. F. *The theory of polymer dynamics*; Clarendon Press: Oxford, 1989.

(43) Borue, V. Yu.; Eruchimovich, I. Y. *Macromolecules* **1990**, *23*, 3625−3632.

induces charge density oscillations of smaller magnitude ($f\Delta\rho$). The 1-D charge density wave formed in a multilayered film can be viewed as a system of parallel plate capacitors whose plates carry charge $Q_{\pm} \approx \pm ef\Delta\rho Sd$, have area S, and are separated by a distance d. The electrostatic energy of such a parallel plate capacitor is

$$U_{cap}/k_BT \approx Sl_B(f\Delta\rho)^2d^3 \tag{A.2}$$

The optimal length scale of the density oscillation is obtained by minimizing polymeric and electrostatic contributions to the film free energy per period

$$\frac{F(d)}{k_BT} \approx S\Delta\rho^2\left(\frac{\sigma^2}{\rho d} + l_Bf^2d^3\right) \tag{A.3}$$

with respect to the period of oscillations, d. This leads to

$$d \approx (\sigma^2/\rho l_Bf^2)^{1/4} \approx \begin{cases} \sigma u^{-1/6}f^{-1/3} \text{ for systems A and B} \\ \sigma u^{-1/4}f^{-1/2} \text{ for systems C and D} \end{cases} \tag{A.4}$$

Thus, the period of density oscillations inside zone II increases with decreasing fraction of charged monomers on the polymer backbone as $f^{-1/3}$ for systems A and B and as $f^{-1/2}$ for systems C and D and decreases with increasing strength of the electrostatic interactions, the value of the parameter u.

The surface overcharging during each deposition step can be evaluated by using the following simple scaling arguments. During each deposition step (excluding the initial layer growth where the polymer surface coverage is controlled by the interactions with the adsorbing substrate), the growing polymeric film is overcharged by the amount $|\Delta Q| \approx ef\Delta\rho Sd$ (excess charge of zone III). This excess charge is screened by counterions on a length scale on the order of the Debye screening length, r_D. The excess charge, ΔQ, and the neutralizing diffusive layer of counterions can be viewed as a parallel plate capacitor with a gap size on the order of the Debye screening length. The electrostatic energy of such a capacitor is equal to

$$\frac{U_{III}}{k_BT} \approx \frac{l_B(f\Delta\rho dS)^2r_D}{S} \approx l_B(f\Delta\rho d)^2Sr_D \tag{A.5}$$

The energy of electrostatic repulsion per excess charged monomer within the overcharged region is estimated as

$$\frac{U_m}{k_BT} \approx \frac{1}{f\Delta\rho dS}\frac{U_{III}}{k_BT} \approx l_Bf\Delta\rho dr_D \tag{A.6}$$

For a polymer chain with N_p monomers the total energy of a chain in this overcharged region is equal to the sum of the repulsive energy, fN_pU_m, and chain cohesive energy, $-k_BTN_p\epsilon_{coh}$, which is due to interaction between a chain and its surroundings. The cohesive energy depends on the strength of the electrostatic and LJ interactions. For systems A and B, the attraction between oppositely charged chains is controlled by correlation/fluctuation-induced attractive interactions and the chain cohesive energy is on the order of the thermal energy, k_BT, per correlation blob, $-k_BTN_p/g \approx -k_BTN_p(uf^2)^{2/3}$. For systems B and C there are two contributions to the chain cohesive energy. The first one is due to short-range attractive LJ interactions, and the other one is due to electrostatic interactions. The first contribution is proportional to $-k_BTN_p\epsilon_{LJ}$, and the electrostatic contribution is on the order of the energy of electrostatic attraction between oppositely charged monomers separated by a typical distance $(f\rho)^{-1/3} \approx \sigma f^{-1/3}$ that can be estimated as $-k_BTN_pfl_B/(f\rho)^{-1/3} \approx -k_BTN_puf^{4/3}$. Note that all evaluations of the cohesive energy are done on the scaling level up to a numerical prefactor.

Chain adsorption leading to surface overcharging ceases to occur when the energy of a chain with N_p monomers inside the overcharged region, $k_BTN_pU_m - k_BTN_p\epsilon_{coh}$, becomes comparable (in order of magnitude) to the same chain's energy in a solution, $k_BTN_p\epsilon_{sol}$. Note that in the framework of the scaling model of a polyelectrolyte the energy per monomer in dilute solution, ϵ_{sol}, is on the order of $(uf^2)^{2/3}$. Thus, the rate of change in the polymer surface coverage, $\Delta\Gamma \approx \Delta\rho d$, is equal to

$$\Delta\Gamma \approx \frac{(\epsilon_{coh} + \epsilon_{sol})}{f^2l_Br_D} \propto f^{-3/2}u^{-1/2}\begin{cases} (uf^2)^{2/3} \text{ for systems A and B} \\ \epsilon_{LJ} + uf^{4/3} \text{ for systems C and D} \end{cases} \tag{A.7}$$

where $r_D \approx (4\pi l_Bfc)^{-1/2}$ is the Debye radius and c is the original monomer concentration in the simulation box.

LA061658E